Available online at www.sciencedirect.com

ScienceDirect

Physics Procedia 00 (2011) 000–000

Physics Procedia

www.elsevier.com/locate/procedia

Technology and Instrumentation in Particle Physics 2011

Revealing the Correlations between Growth Recipe and Microscopic Structure of Bi-alkali/Multi-alkali Photocathodes

S. W. Lee[a]*, K. Attenkofer[a], M. Demarteau[a], J. Smedley[b], I. Ben-Zvi[b], T. Rao[b], M. Ruiz-Oses[c], X. Liang[c], E. M. Muller[c], H. Padmore[d], T. Vecchione[d]

[a]*Argonne National Laboratory, 9700 S. Cass Ave., Argonne, IL, 60439, USA*
[b]*Brookhaven National Laboratory, P.O.Box 5000, Upton, NY, 11973, USA*
[c]*Stony Brook University, Stony Brook, NY, USA*
[d]*Lawrence Berkeley National Laboratory, USA*

Abstract

For the development of high quantum efficiency photocathodes, the multialkali photocathode growth process was studied through in-situ X-ray scattering measurements, including X-ray diffractometry (XRD) and X-ray reflectometry (XRR). Characterization during real-time growth revealed correlations between growth parameters and microscopic structural change of the photocathode. This paper presents preliminary results of an ongoing experiment to understand the growth mechanism. X-ray diffractometry enabled the observation of selective growth of specific crystalline orientation during the deposition and evaporation of an Sb layer. A phase transition of the Sb layer was also measured. X-ray reflectometry revealed surface roughness changes during the growth process and permitted layer thickness measurements while the K layer was evaporated on an ex-situ grown Sb layer, in addition to in-situ Sb layer growth.

Keywords: Multi-alkali photocathode; thin film growth; X-ray diffractometry; X-ray reflectometry

1. Motivation

Multi-alkali photocathodes are widely produced cathodes in industry. They are grown in cost-effective thin-film technology permitting the use of a wide range of amorphous and polycrystalline substrates. In

* Corresponding author. Tel.: +1-201-602-9004
E-mail address: seon.w.lee@gmail.com.

industry, however, photocathodes are grown in a glass phototube and sealed in vacuum. The details of the growth mechanism of photocathodes such as structural formation, chemical compositions, cathode thickness, surface roughness and their relation between overall quantum efficiency are poorly understood. Argonne National Laboratory aims to develop a high quantum efficiency bi-alkali/multi-alkali photocathode for an 8" x 8" large-area photocathode for industrialization. Brookhaven National Laboratory, Stony Brook University and Lawrence Berkeley National Laboratory are collaborating for an accelerator application. It is critical to understand how the growth parameters affect the overall quantum efficiency to enable the development of an optimized reproducible recipe for high quantum efficiency photocathode production. Often, the growth process parameters are chosen by heuristically optimized recipes which typically are proprietary. The resulting quantum efficiency of the detection devices varies widely from 20% to 25% for typical detector systems and is up to 42% for newly developed high QE detectors. Even quantum efficiencies of up to 60% were reported for one-of-a-kind cathode-systems. Our goal is to explain these variations by cross-correlating the microscopic and chemical compositions of the cathode film with the individual process steps and ultimately to develop a theory-inspired growth recipe which results in high quantum efficiency, wavelength tunability, and is compatible with conventional process technology in industry. In-situ X-ray scattering measurement is a suitable way to analyze the correlation between growth recipe, structure of the cathode and quantum efficiency. In this paper, we present partial results of our experiment on the growth process from in-situ K_2CsSb growth and real-time X-ray scattering measurement at the National Synchrotron Light Source (NSLS) at Brookhaven National Laboratory.

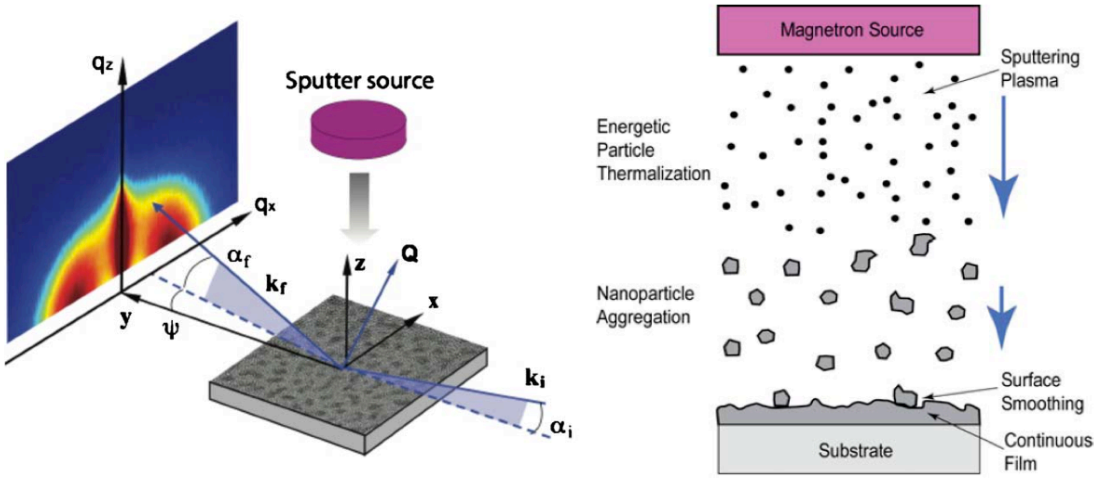

(a) (b)

Figure 1. (a) In-situ X-ray scattering measurements. Q is the wave vector transfer, the difference between incident wave vector k_i and scattered wave vector k_f. ψ is an in-plane angle with respect to *y* direction. α_i is the incident angle and α_f is the scattering angle with respect to the surface of the sample [1,2]. (b) The schematic of the growth of multi-alkali photocathodes.

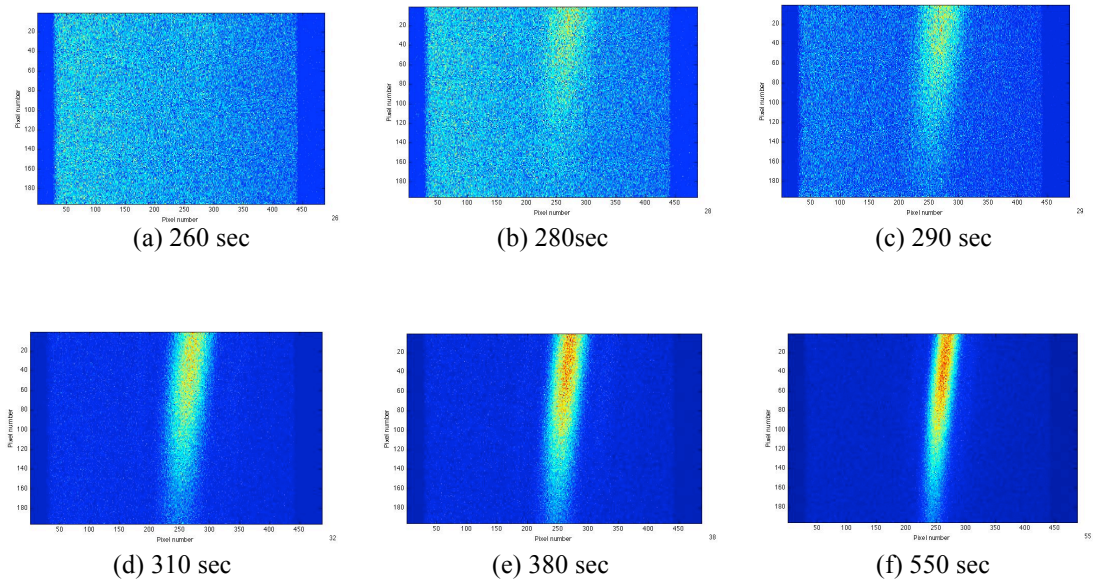

(a) 260 sec (b) 280sec (c) 290 sec

(d) 310 sec (e) 380 sec (f) 550 sec

Figure 2. Selected real-time X-ray diffraction patterns recorded during in-situ Sb layer deposition (total thickness of 40nm) for 1440 secs. Images were taken every 10 secs. X and Y axis are pixel numbers. (a) before start to do evaporation (b), (c) weak and broad peak appears (d), (e), (f) becomes stronger and sharper, indicating the crystallization of the Sb layer.

2. Experimental Details

To achieve high quantum efficiency photocathode growth recipes, it is essential to visualize the microscopic structure, chemical composition, and speciation of the film during the growth in real time. Using an in-situ X-ray diffractometry (XRD) setup, we are able to analyze the crystal structure of the film, e.g. the identification of coexisting crystalline phases, their quantitative analysis, the determination of the crystallite sizes, and a preferential growth or texture if existent. By combining state-of-the-art detector technology and high flux X-ray beamlines at synchrotrons we are not only able to achieve a time resolution of 100ms or better but also perform grazing incidence techniques which allow a depth probe of the film. The achieved data quality in combination with the time resolution allow us to characterize all changes inside the cathode during the processing, including inter-diffusion of the alkali metals into the Sb matrix, the solid state reactions of the alkalis with the Sb to the different inter-metallic compounds and to determine the individual time constants of these processes.

In-situ growth and real-time X-ray scattering measurements were performed at the X21 beamline of the NSLS. The energy of the monochromatic X-ray beam was 10 KeV (λ = 1.2398 Å) with approximately $2x10^{12}$ photons/s flux after a Si(111) crystal monochromator. The base pressure of the ultra high vacuum growth chamber was 10^{-9} Torr [1,3]. Pilatus 100K detector is used to take data. Pixel size is 172 x 172 μm^2. Image format is 487x195 (=94,965 pixels). Readout time is 2.7ms.

Two methods have been used to make the measurements: X-ray diffractometry (XRD) and X-ray reflectometry (XRR). By using X-ray diffractometry with a detector with a read-out speed of 2.7ms, one is able to study formation of crystal structure during the growth process. Using X-ray reflectometry, we

measure the thickness of the layer and the surface roughness. By Fourier transformation of fringes, the thickness and the roughness of the layer can be determined.

Figure 1 shows the schematic of the in-situ photocathode growth and real-time X-ray scattering measurements. The texture of the materials during the growth can be studied by in-situ X-ray diffractometry measurement. X-ray reflectometry patterns come along q_z and depend on the electron density of the deposited layer. Fourier transformation of X-ray reflectometry scans give surface roughness and thickness information of a single layer or sum of multi-layers [3,4].

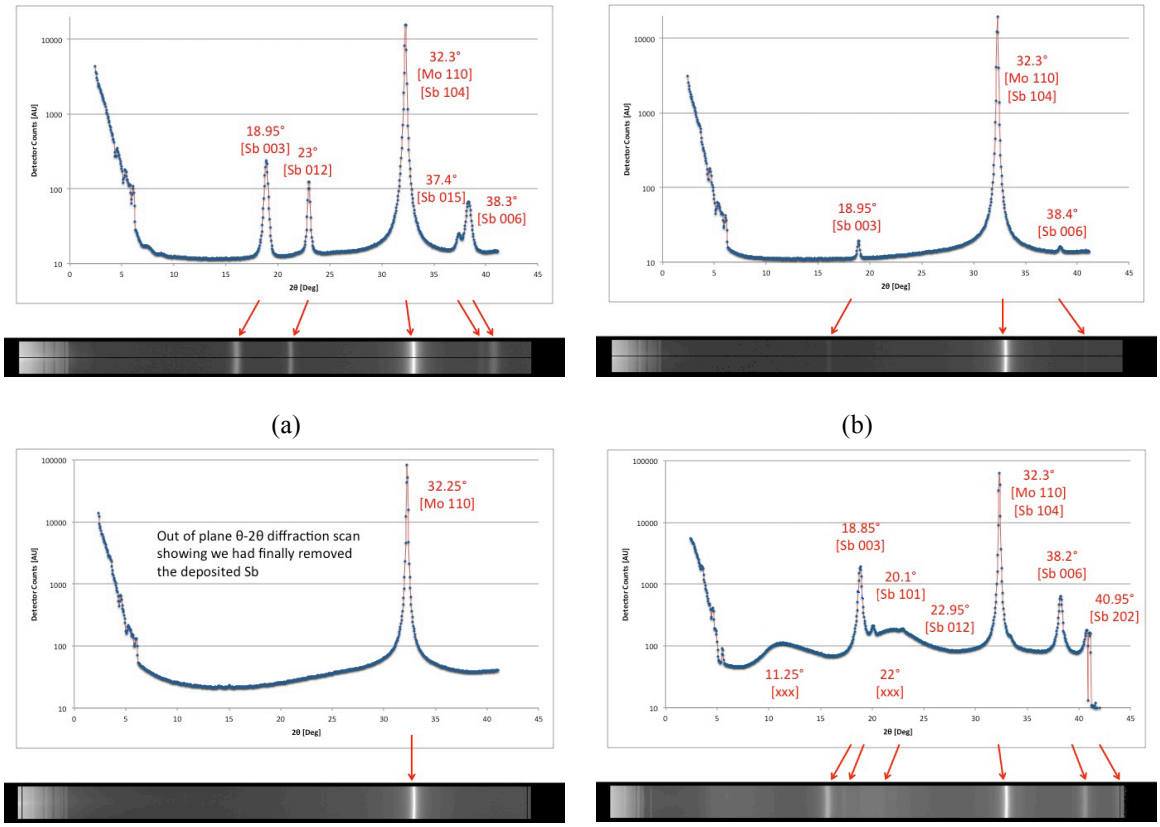

Figure 3. The in-situ X-ray diffraction patterns taken during Sb layer and K_2CsSb growth on a Mo substrate. (a) Sb deposition on Mo substrate (b) Sb layer was evaporated from Mo substrate. Specific orientation of Sb crystalline faces, Sb(003) and Sb(006), left on Mo substrate longer than other orientation of crystalline faces (c) Sb layer was completely removed from Mo substrate (d) X-ray diffraction pattern after growth of K_2CsSb photocathode.

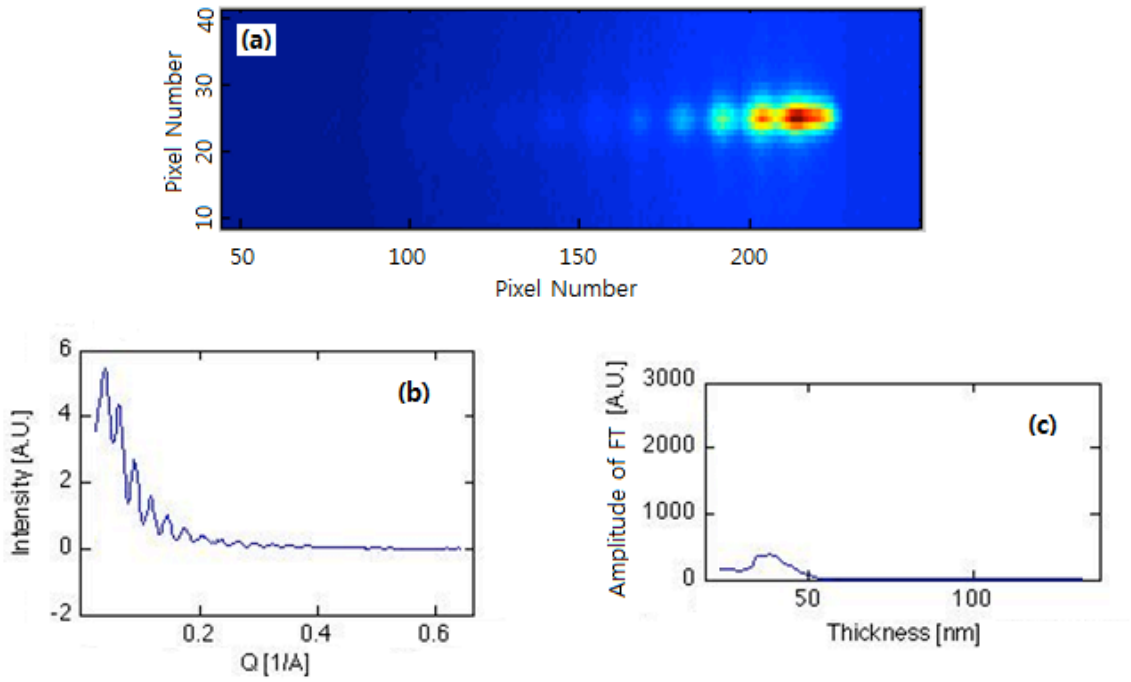

Figure 4. Single frame of X-ray reflectometry measurement from Sb Layer (a) Raw data from the detector (b) Reflectivity curve from Sb layer (c) Fourier transform of specular reflectivity curve. The peak position was 37 nm.

3. Results and Discussion

3.1. X-ray Diffractometry (XRD)

Using in-situ X-ray diffractometry, a phase transition in the Sb layer was measured during deposition in Figure 2. The center of the detector was fixed at 19 degrees (~2θ) to monitor texturing of Sb (003) orientation peak appearing at 2θ =19.015 degree [5]. In the beginning of the deposition, a weak broad peak appears which later becomes sharper and stronger, indicating a phase transition from an amorphous to a crystalline structure. Thickness of layer was monitored by quartz crystal monitor (QCM) in real-time during the deposition and XRD measurement. The diffraction patterns were recorded every 10 seconds for 1440 seconds. The phase transition occurred at a thickness of 7-8 nm, which corresponds to 260~550 seconds. This result was obtained consistently over three depositions of Sb.

Figure 3(a)-(c) shows in-situ diffractometry measurements during the Sb layer deposition and evaporation on a Mo substrate. First, an Sb layer was deposited on a Mo substrate and X-ray diffraction patterns were measured. They show a clear Mo peak and several different crystalline faces of Sb grains as indicated by the other peaks in Figure 3(a). The Sb layer was then evaporated from the Mo substrate. Specific orientations of crystalline faces, Sb(003) and Sb(006), remained on the substrate longer than

other crystalline faces (Figure 3(b)). Finally, all Sb layer was evaporated from Mo substrate (Figure 3(c)). Therefore, this result shows the evidence of selective growth for specific orientation of crystalline faces by repeating the deposition and evaporation process. There is a substantial literature on the change of the work function depending on different crystalline faces [6,7,8]. It would be beneficial to achieve higher quantum efficiency if we can selectively grow specific orientations of crystalline faces that have a lower work function. Figure 3(d) shows the diffraction pattern from a fully grown K_2CsSb photocathode layer. Two broad peaks were observed in addition to the Sb and Mo peaks. It is not clear what the origin of these two broad peaks is. However, we speculate that they are from either a mixture of different chemical compositions of alkali metals or the existence of an amorphous phase.

3.2. X-ray Reflectometry (XRR)

Figure 4 shows a single frame of an X-ray reflectivity scan from the Sb layer. Figure 4(a) is the raw data taken from the detector. Clear fringes are observed. This image from the detector is converted into an intensity versus wave transfer vector, shown in Figure 4(b). The thickness and surface roughness of the Sb layer are determined through a Fourier transformation of the fringes of the specular reflectivity curve (Figure 4(c)). The peak position corresponds to the thickness of the layer. The surface roughness is correlated with the peak broadening [3,9,10]. Real-time X-ray reflectivity was monitored repeatedly during in-situ Sb growth. The total deposited thickness was approximately 30 nm. Fringes were appearing in the range of approximately 15~25nm. We can infer that the Sb layer is forming a thin film with a smooth surface from 15nm to 25nm. After a thickness of 25nm the surface becomes rough since the Sb thin film crystallizes and grows bigger crystalline grains.

Figure 5 is the real-time X-ray reflectivity measurement during K deposition on top of ex-situ grown Sb layer. Figure 5(a) is a measurement of the ex-situ grown Sb layer and shows a thickness of the Sb layer prior to K deposition of about 20nm. As K is deposited on the Sb layer, the thickness increases constantly. The amplitude of the peak, however, becomes smaller because the K is forming islands and the surface is getting rough (Figure 5(b)). During further deposition the peak completely disappears indicating that the the surface becomes very rough (Figure 5(c)). As the K islands get bigger, they start to touch adjacent islands and produce a thin film. At that moment, a peak starts to appear again (Figure 5(d)).

4. Conclusion and future study

From real-time X-ray diffraction measurements, a phase transition was observed from amorphous to crystalline for the thickness of 7~8 nm during Sb layer growth. Therefore, different thickness of Sb layer must be deposited below and over 7~8 nm to justify the effect for the quantum efficiency. We have observed the evidence of selective growth of specific orientation crystalline grains by repeating the deposition and evaporation of Sb layer. If we can selectively grow crystalline faces, which have lower work function, it could lead to increasing the quantum efficiency. In-situ Sb layer growth and K deposition on ex-situ grown Sb layer was monitored by real-time X-ray reflectivity measurement. We have learned that surface of the Sb layer becomes rough after approximately 25 nm. Also surface roughness changes during the K deposition. Based on these results, surface roughness can possibly be modified.

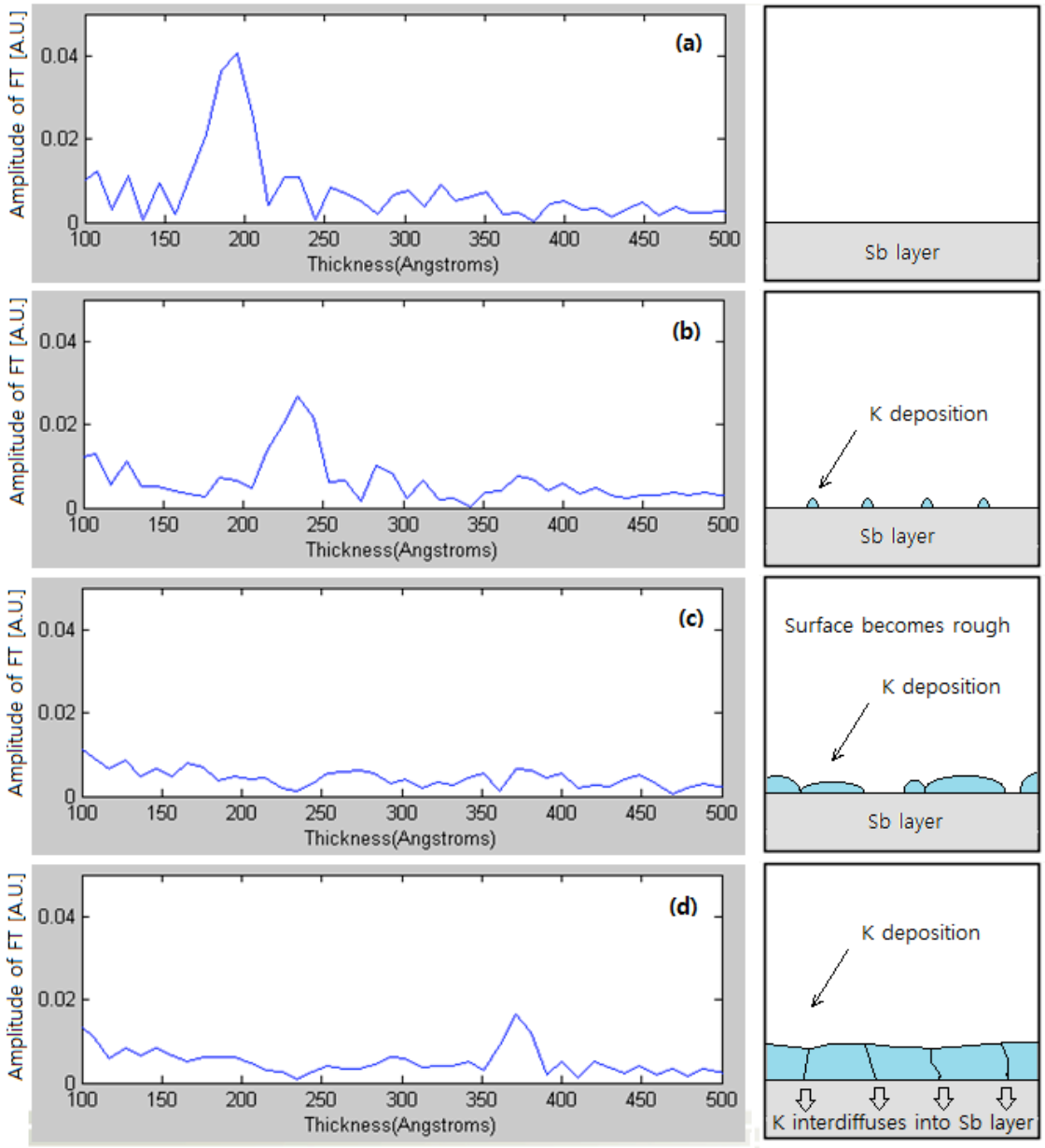

Figure 5. Real-time X-ray reflectivity measurement during K_2CsSb photocathode growth on top of an ex-situ grown Sb layer (a) Sb layer was grown ex-situ before K deposition (b) Peak reduces as K is deposited and forms islands (c) Peak disappears when surface becomes very rough by forming K cluster (d) During further deposition, islands of deposited K grow bigger, meet adjacent islands, K starts to form a thin film and fringes start to appear again.

Acknowledgements

The submitted manuscript has been created by UChicago Argonne, LLC, Operator of Argonne National Laboratory ("Argonne"). Argonne, a U.S. Department of Energy Office of Science laboratory, is operated under Contract No. DE-AC02-06CH11357. The U.S. Government retains for itself, and others acting on its behalf, a paid-up nonexclusive, irrevocable worldwide license in said article to reproduce, prepare derivative works, distribute copies to the public, and perform publicly and display publicly, by or on behalf of the Government.

References

[1] L. Zhou, Y. Wang, H. Zhou, M. Li, R. L. Headrick, Phy. Rev. B 82, 075408 (2010)

[2] https://indico.bnl.gov/getFile.py/access?contribId=8&sessionId=2&resId=0&materialId=slides&confId=290, *Photocathode Physics for Photoinjectors Workshop at Brookhaven National Laboratory* (2010)

[3] Y. Wang, H. Zhou, L. Zhou, R. L. Headrick, J. Appl. Phys. 101, 023503 (2007)

[4] B. Poust, R. Sandhu, M. Goorsky, Phys. Status Solidi A 206, No. 8, 1780-1784 (2009)

[5] JCPDS-International Center for Diffraction Data (1998)

[6] Hopkins, B. J., and K. R. Pender, Brit. J. Appl. Phys., 17, 281 (1966)

[7] Mendenhall, C. E., and C. F. DeVoe, Phys. Rev., 51, 346 (1937)

[8] A. H. Sommer, *Photoemissive Materials, John Wiley & Sons, Inc*. (1968)

[9] P. Colombi, D. K. Agnihotri, V. E. Asadchikov, E. Bontempi, D. K. Bowen, C. H. Chang, L. E. Depero, M. Farnworth, T. Fujimoto, A. Gibaud, M. Jergel, M. Krumrey, T. A. Lafford, A. Lamperti, T. Ma, R. J. Matyi, M. Meduna, S. Milita, K. Sakurai, L. Shabelnikov, A. Ulyanenkov, A. Van der Lee, C. Wiemer, *J. Appl. Cryst.* 41, 143-152 (2008)

[10] E. Smigiel, A. Cornet, *J. Phys. D: Appl. Phys*. 33, 1757-1763 (2000)